2026 IEEE/SICE International Symposium on System Integration (SII)
January 11-14, 2026. Cancún, México

State Estimation and Linear Discrete Model Predictive Control for the Hydration Process in a Lime-Based Thermochemical Energy Storage System*

Anja Rentz[1], Venizelos E. Sourmelis T.[2], Viktor Kühl[2], Matthias Schmidt[2], Marc Linder[3], Oliver Sawodny[1]

***Abstract*— Thermochemical energy storage based on the reversible reaction of CaO and H_2O to $Ca(OH)_2$ is a promising solution for sustainable storage of excessive renewable energy. For efficient and safe discharge of the system (hydration of CaO), a control strategy is necessary. Starting from a nonlinear dynamic model, the system is linearized and discretized to enable the design of a Kalman filter for state estimation and a Model Predictive Controller (MPC). Simulation results demonstrate that the Kalman filter provides accurate state reconstruction and effectively filters measurement noise from the system outputs. Four different MPC objectives, targeting key temperatures and thermal power, are evaluated. All variants show good tracking performance and are suitable for real-time application. A comparison between the linear discrete-time MPC with state estimation and a nonlinear continuous-time MPC with full state information reveals no significant performance loss, while achieving a reduction in computation time.**

I. INTRODUCTION

Worldwide, $63\,\%$ of heating power for buildings is provided by fossil fuels, with natural gas accounting for $42\,\%$ [1]. This indicates significant potential for emission reductions in the heating sector. Electrification, particularly through heat pumps, is a promising solution, yet increases dependence on intermittent renewable electricity from the grid. Heating demand, however, must be met continuously, regardless of daily or seasonal availability.

Energy storage systems in households and grid infrastructure help buffer these fluctuations, but long-term storage remains a challenge. Thermochemical energy storage (TCES) offers a loss-free solution for both short- and long-term applications. This work examines a lime-based TCES employing the recyclable materials calcium oxide (CaO) and calcium hydroxide ($Ca(OH)_2$). The reversible reaction $CaO + H_2O \underset{endo.}{\overset{exo.}{\rightleftharpoons}} Ca(OH)_2 + \Delta H$, with ΔH representing the reaction enthalpy, is used for energy storage (charge, dehydration) and release (discharge, hydration). In between, the energy is stored in the chemical bonds. For technical details and experimental studies refer to [2][3].

The hydration process involves fast reaction times and temperature boundaries, that have to be respected for safe operation. Due to the system's multivariable nature, time delays and the constrained operational range, advanced control strategies are required to handle the system effectively.

Model Predictive Control (MPC) has been popular in chemical process control due to its ability to handle MIMO (multiple input, multiple output) systems and operational constraints. Early applications to batch and continuous reactors demonstrated its advantages over traditional control approaches, particularly in predictive accuracy and constraint handling [4][5]. In real-world process applications, some internal system variables, such as concentrations or internal temperatures, are not directly measurable. This makes state estimation an essential component for the practical implementation of MPC.

The Kalman filter is a commonly used method for state estimation in dynamic systems. In contrast to simpler observers such as the Luenberger observer, it explicitly accounts for process and measurement noise. Compared to more computationally intensive approaches like Moving Horizon Estimation, the Kalman filter offers a recursive solution without requiring the repeated solution of an optimization problem.

Since its introduction in 1960 [6], several extensions have been developed, such as the Extended Kalman Filter (EKF). Algorithmic details for both the standard and EKF formulations are summarized in [7].

Applications of Kalman filtering in chemical batch and semi-batch processes date back to early works such as [8], [9]. A comprehensive investigation was presented in [10], applying EKF to the Tennessee Eastman Challenge Process, a nonlinear plant involving four unit operations and multiple chemical conversions.

In practice, MPC and Kalman filters are commonly used together. In [12], EKF-based state estimation was implemented together with linear MPC for a pulp digester. [13] applied EKF with NMPC for semi-batch polymerization, using a reduced-order model and validating results experimentally. The application of MPC and a multi-rate EKF for distillation in [14] demonstrates feasibility in real-time operation. More recently, [15] evaluated NMPC for a semi-batch CSTR, with EKF-based state estimation.

Our first work on the hydration process in this TCES application covered the modeling process as well as first

*Funded by the Deutsche Forschungsgemeinschaft (DFG, German Research Foundation) - Project-ID 279064222 - SFB 1244, A05 and the Deutsche Forschungsgemeinschaft (DFG) under Germany's Excellence Strategy - EXC 2120/1 - 390831618.

[1]A. Rentz and O. Sawodny are with the Institute for System Dynamics, University of Stuttgart, Waldburgstr. 19, 70563 Stuttgart, Germany {rentz, sawodny}@isys.uni-stuttgart.de

[2]V. E. Sourmelis T., V. Kühl and M. Schmidt are with the German Aerospace Center (DLR), Linder Höhe, 51147 Cologne, Germany {Venizelos.SourmelisTerzopoulos,Viktor.Kuehl, Matthias.Schmidt}@dlr.de

[3]M. Linder is with the German Aerospace Center (DLR), Pfaffenwaldring 38-40, 70569 Stuttgart, Germany Marc.Linder@dlr.de

Fig. 1: Experimental setup for hydration of CaO with storage silo Ⓐ, buffer storage Ⓑ, motor Ⓒ and the reactor (left). View into the reactor (right) [11].

approaches for system identification [16]. In subsequent work [11], we have identified time delays in the nonlinear system dynamics and designed a nonlinear model predictive controller under consideration of different control objectives.

However, the nonlinear MPC has been designed under assumption of full state knowledge. For application to our experimental setup, a state observer has to reconstruct the full state information.

Therefore, the main contribution of this work is the design of a Kalman filter for the lime storage system. For this, a linearized, time-discretized model of the system is derived from the nonlinear model equations. The full state information is then used for MPC, employing the linearized discrete system model. This reduces computational complexity but also offers practical advantages for implementation to the experimental setup.

This paper is structured as follows. Section II introduces the experimental setup and the nonlinear model equations along with the derivation of the linearized, time-discrete model equations. Sections III and IV describe the design process for Kalman filter and MPC. In Section V, results for observer and MPC performance are evaluated and discussed. Finally, Section VI concludes this work and gives an outlook.

II. Experimental Setup and Model Equations

The experimental setup (Figs. 1, 2) remains unchanged from the description in [11]. While Table I lists all components and measurements, a detailed description of the setup can be found in [11]. The experimental procedure comprises the transport of a CaO batch into the reactor, pulsed water injection to initiate and sustain the reaction, and heat extraction through the cooling water in the coil.

TABLE I: Components and sensors of the experimental setup.

Comp.	Description	Sens.	Description
Ⓐ	Storage silo	ⓐ	Thermocouple (Type K, 3-Point)
Ⓑ	Buffer storage	ⓑ	Thermocouple (Type K)
Ⓒ	Motor	ⓒ	Thermocouple (Type K)
Ⓓ	Reactor hull	ⓓ	Flow rate meas. (inline flow)
Ⓔ	Plowshare mixing tool	ⓔ	Flow rate meas. (paddle wheel)
Ⓕ	Reactor water injection	ⓕ	Thermocouple (Type K)
Ⓖ	Vacuum transport tube		
Ⓗ	Cooling coil		
Ⓘ	Circulating pump		
Ⓚ	Magnetic Valve		

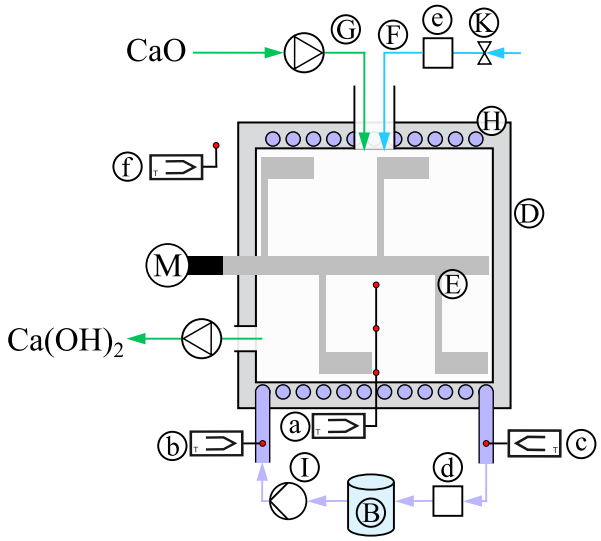

Fig. 2: Side view of the reactor system with components and measurements [11].

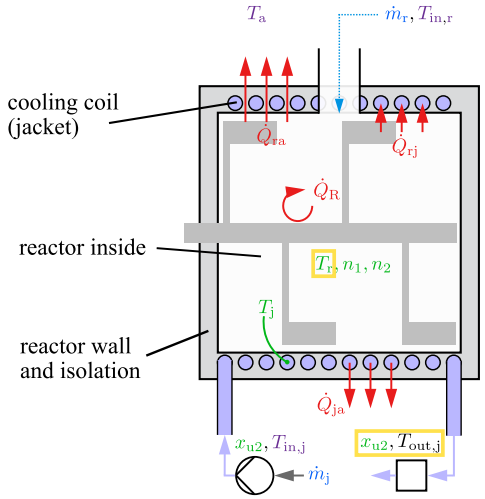

Fig. 3: Model of the reactor during hydration. Green: states, blue: inputs, purple: disturbance, yellow box: outputs.

The system model was first derived and identified in [16] and subsequently refined to match the experimental setup (Fig. 1). For completeness, the model equations and algebraic relations are summarized in this section. The model is based on mass and enthalpy balances combined with reaction kinetics, capturing all relevant effects shown in Fig. 3.

Indices and parameter values are listed in Tabs. II-III. As in previous work, index j denotes the cooling water circuit, referencing the earlier setup with a jacket-like pillow plate heat exchanger.

The system states are the reactor temperature T_r, cooling water temperature T_j, substance amounts n_1 (CaO), n_2 (H_2O) and the cooling water mass flow x_{u2}. Inputs are the water mass flow of reactor injection $\dot{m}_r$ and the desired cooling water mass flow $\dot{m}_j$. Disturbances include the

TABLE II: Subscripts used for modeling.

Sub.	Description	Sub.	Description
j	cooling coil (jacket)	1	CaO
r	reactor	2	H_2O
a	ambiance	3	$Ca(OH)_2$
cn	additional heat capacities and masses		

ambient temperature T_a and temperatures at reactor inlet $T_\mathrm{in,r}$ and cooling coil inlet $T_\mathrm{in,j}$. The nonlinear model equations are

$$\begin{aligned}\dot{T}_\mathrm{r} =& C_\mathrm{r}^{-1}\big[\underbrace{\Delta H R(n_1,n_2)}_{=:\dot{Q}_\mathrm{R}} + \frac{\dot{m}_\mathrm{r}}{M_2} c_{\mathrm{p},2}\,(T_\mathrm{in,r} - T_\mathrm{r}) \\ & - \underbrace{A_\mathrm{rj} U_\mathrm{rj}\,(T_\mathrm{r} - T_\mathrm{j})}_{=:\dot{Q}_\mathrm{rj}} - \underbrace{A_\mathrm{ra} U_\mathrm{ra}\,(T_\mathrm{r} - T_\mathrm{a})}_{=:\dot{Q}_\mathrm{ra}} \\ & + (c_{\mathrm{p},1} + c_{\mathrm{p},2} - c_{\mathrm{p},3})\,R(n_1,n_2) T_\mathrm{r}\big], \end{aligned} \tag{1a}$$

$$\begin{aligned}\dot{T}_\mathrm{j} =& C_\mathrm{j}^{-1}\big[c_\mathrm{p,j}\,(2T_\mathrm{in,j} - 2T_\mathrm{j})\,x_\mathrm{u2} \\ & + \underbrace{A_\mathrm{rj} U_\mathrm{rj}\,(T_\mathrm{r} - T_\mathrm{j})}_{=:\dot{Q}_\mathrm{rj}} - \underbrace{A_\mathrm{ja} U_\mathrm{ja}\,(T_\mathrm{j} - T_\mathrm{a})}_{=:\dot{Q}_\mathrm{ja}}\big], \end{aligned} \tag{1b}$$

$$\dot{n}_1 = -R(n_1,n_2), \tag{1c}$$

$$\dot{n}_2 = -R(n_1,n_2) + \frac{\dot{m}_\mathrm{r}}{M_2}, \tag{1d}$$

$$\dot{x}_\mathrm{u2} = \frac{1}{T}\left(K\dot{m}_\mathrm{j} - x_\mathrm{u2}\right). \tag{1e}$$

Here, $\dot{Q}_\mathrm{R}$ denotes the heat of reaction, $\dot{Q}_\mathrm{rj}$ the heat transfer to the cooling water, and $\dot{Q}_\mathrm{ra}$ and $\dot{Q}_\mathrm{ja}$ the thermal losses to the environment. Additional algebraic relations are

$$R(n_1,n_2) = k\frac{(n_1 - 0.05\,(n_{1,0} + n_{3,0}))\,n_2}{V_\mathrm{r}}, \tag{2}$$

$$\Delta H = -\left(-H_1 - H_2 + H_3\right), \tag{3}$$

$$C_\mathrm{r} = c_{\mathrm{p},1} n_1 + c_{\mathrm{p},2} n_2 + c_{\mathrm{p},3}\underbrace{(n_{1,0} + n_{3,0} - n_1)}_{=n_3} + c_\mathrm{cn,r}, \tag{4}$$

$$C_\mathrm{j} = V_\mathrm{j}\rho_2 c_\mathrm{p,j} + c_\mathrm{cn,j}, \tag{5}$$

characterizing the reaction rate R, the reaction enthalpy ΔH and the heat capacities of reactor C_r and cooling coil C_j.

The cooling water outlet temperature $T_\mathrm{out,j}$ is assumed as

$$T_\mathrm{out,j} = 2T_\mathrm{j} - T_\mathrm{in,j}. \tag{6}$$

With this, the system output power is computed

$$P = x_\mathrm{u2} c_\mathrm{p,j}\,(T_\mathrm{out,j} - T_\mathrm{in,j}) = x_\mathrm{u2} c_\mathrm{p,j}\,2\,(T_\mathrm{j} - T_\mathrm{in,j}), \tag{7}$$

with the specific heat capacity of water $c_\mathrm{p,j}$.

The system state $\boldsymbol{x}$, system input $\boldsymbol{u}$, disturbance $\boldsymbol{v}$, and system output $\boldsymbol{y}$ are

$$\boldsymbol{x} = [T_\mathrm{r}, T_\mathrm{j}, n_1, n_2, x_\mathrm{u2}]^\mathrm{T}, \tag{8a}$$

$$\boldsymbol{u} = [\dot{m}_\mathrm{r}, \dot{m}_\mathrm{j}]^\mathrm{T}, \tag{8b}$$

$$\boldsymbol{v} = [T_\mathrm{a}, T_\mathrm{in,r}, T_\mathrm{in,j}]^\mathrm{T}, \tag{8c}$$

$$\boldsymbol{y} = [T_\mathrm{r}, T_\mathrm{out,j}, x_\mathrm{u2}]^\mathrm{T}. \tag{8d}$$

The state x_u2 has been included into the system output following experimental identification of the pump dynamic in [11]. This yields the nonlinear MIMO system

$$\dot{\boldsymbol{x}}(t) = \boldsymbol{f}(\boldsymbol{x}(t), \boldsymbol{u}(t), \boldsymbol{v}(t)), \tag{9a}$$

$$\boldsymbol{x}(0) = \boldsymbol{x_0}, \tag{9b}$$

$$\boldsymbol{y}(t) = \boldsymbol{C}\boldsymbol{x}(t) + \boldsymbol{D}_\mathrm{v}\boldsymbol{v}(t), \tag{9c}$$

$$\boldsymbol{C} = \begin{bmatrix}1&0&0&0&0\\0&2&0&0&0\\0&0&0&0&1\end{bmatrix}, \quad \boldsymbol{D}_\mathrm{v} = \begin{bmatrix}0\\-1\\0\end{bmatrix}. \tag{9d}$$

TABLE III: Parameters and values. The upper range of parameters is from literature, the middle ones are measured, bottom range is identified [11].

Par.	Description	Value	Unit
$c_{\mathrm{p},1}$	molar heat capacity CaO	42.09	$\mathrm{J/(mol\,K)}$
$c_{\mathrm{p},2}$	molar heat capacity H_2O	75.38	$\mathrm{J/(mol\,K)}$
$c_{\mathrm{p},3}$	molar heat capacity $Ca(OH)_2$	87.45	$\mathrm{J/(kg\,K)}$
$c_\mathrm{p,j}$	specific heat capacity H_2O	4190	$\mathrm{J/(kg\,K)}$
H_1	std. enthalpy of form. CaO	-635.09	kJ/mol
H_2	std. enthalpy of form. H_2O	-285.8	kJ/mol
H_3	std. enthalpy of form. $Ca(OH)_2$	-986.09	kJ/mol
M_2	molar mass H_2O	18.02×10^{-3}	kg/mol
ρ_2	density of water	997	$\mathrm{kg/m^3}$
A_rj	heat transfer area r to j	0.223	$\mathrm{m^2}$
A_ra	heat transfer area r to amb.	0.223	$\mathrm{m^2}$
A_ja	heat transfer area j to amb.	0.223	$\mathrm{m^2}$
V_r	reactor volume	19.5	l
V_j	jacket volume	674	ml
U_rj	Thermal transmittance r to j	147.60	$\mathrm{W/(m^2\,K)}$
U_ra	Thermal transm. r to amb.	2×10^{-14}	$\mathrm{W/(m^2\,K)}$
U_ja	Thermal transm. j to amb.	35.42	$\mathrm{W/(m^2\,K)}$
$c_\mathrm{cn,r}$	Additional thermal masses r	4.23	kJ/K
$c_\mathrm{cn,j}$	Additional thermal masses j	7.37	kJ/K
k	Reaction rate coefficient	3.74×10^{-5}	$\mathrm{m^3/(mol\,s)}$
K	Pump dynamic amplification	1.04	$-$
T	Pump dynamic time constant	3.91	s
$t_\mathrm{d,r}$	Input time delay r injection	5	s
$t_\mathrm{d,j}$	Input time delay cooling water	2	s

The input delays $t_\mathrm{d,r}$ (reactor injection) and $t_\mathrm{d,j}$ (cooling water flow), identified in [11], are incorporated after linearization.

A. Linearized Model Equations

The nonlinear system (9) is first linearized and then discretized. Linearization enables the application of Kalman filter and the reformulation of MPC as a quadratic optimization problem. The linearized model is

$$\begin{aligned}\dot{\boldsymbol{x}}(t) =& \boldsymbol{A}\boldsymbol{x}(t) + \boldsymbol{B}_\mathrm{u}\boldsymbol{u}(t) + \boldsymbol{B}_\mathrm{v}\boldsymbol{v}(t) \\ & + \boldsymbol{f}(\boldsymbol{x}_\mathrm{L}, \boldsymbol{u}_\mathrm{L}, \boldsymbol{v}_\mathrm{L}) - \boldsymbol{A}\boldsymbol{x}_\mathrm{L} - \boldsymbol{B}_\mathrm{u}\boldsymbol{u}_\mathrm{L} - \boldsymbol{B}_\mathrm{v}\boldsymbol{v}_\mathrm{L}, \end{aligned} \tag{10a}$$

$$\boldsymbol{x}(0) = \boldsymbol{x_0}, \tag{10b}$$

$$\boldsymbol{y}(t) = \boldsymbol{C}\boldsymbol{x}(t) + \boldsymbol{D}_\mathrm{v}\boldsymbol{v}(t), \tag{10c}$$

$$\begin{aligned}\boldsymbol{A} &= \left.\frac{\partial \boldsymbol{f}}{\partial \boldsymbol{x}}\right|_{(\boldsymbol{x}_\mathrm{L}, \boldsymbol{u}_\mathrm{L}, \boldsymbol{v}_\mathrm{L})}, \quad \boldsymbol{B}_\mathrm{u} = \left.\frac{\partial \boldsymbol{f}}{\partial \boldsymbol{u}}\right|_{(\boldsymbol{x}_\mathrm{L}, \boldsymbol{u}_\mathrm{L}, \boldsymbol{v}_\mathrm{L})}, \\ \boldsymbol{B}_\mathrm{v} &= \left.\frac{\partial \boldsymbol{f}}{\partial \boldsymbol{v}}\right|_{(\boldsymbol{x}_\mathrm{L}, \boldsymbol{u}_\mathrm{L}, \boldsymbol{v}_\mathrm{L})}. \end{aligned} \tag{10d}$$

The linearization operating point $(\boldsymbol{x}_\mathrm{L}, \boldsymbol{u}_\mathrm{L}, \boldsymbol{v}_\mathrm{L})$ may require regular updates to maintain model quality.

B. Discretization of the Model Equations

For discretization, the explicit Euler method is chosen due to its computational efficiency, since for every update of the linearization point, the matrices of the linear dicrete-time model have to be recomputed. Approximating the state derivative at discrete times $t = k\Delta t$ with $k = 0, 1, ..$ and sampling time Δt leads to the discrete system dynamic

$$\begin{aligned}\boldsymbol{x}_{k+1} =& \boldsymbol{A}_\mathrm{d}\boldsymbol{x}_k + \boldsymbol{B}_\mathrm{u,d}\boldsymbol{u}_k + \boldsymbol{B}_\mathrm{v,d}\boldsymbol{v}_k \\ & \underbrace{+\boldsymbol{f}_\mathrm{d} - \boldsymbol{A}_\mathrm{d,L}\boldsymbol{x}_\mathrm{L} - \boldsymbol{B}_\mathrm{u,d}\boldsymbol{u}_\mathrm{L} - \boldsymbol{B}_\mathrm{v,d}\boldsymbol{v}_\mathrm{L}}_{=:\boldsymbol{F}(\boldsymbol{x}_\mathrm{L}, \boldsymbol{u}_\mathrm{L}, \boldsymbol{v}_\mathrm{L})}, \end{aligned} \tag{11}$$

with $\boldsymbol{A}_\mathrm{d} = (\boldsymbol{I}_x + \Delta t\boldsymbol{A})$, identity matrix $\boldsymbol{I}_x$ of dimension x, $\boldsymbol{B}_\mathrm{u,d} = \Delta t\boldsymbol{B}_\mathrm{u}$, $\boldsymbol{B}_\mathrm{v,d} = \Delta t\boldsymbol{B}_\mathrm{v}$, $\boldsymbol{A}_\mathrm{d,L} = \Delta t\boldsymbol{A}$ and $\boldsymbol{f}_\mathrm{d} = \Delta t\boldsymbol{f}(\boldsymbol{x}_\mathrm{L}, \boldsymbol{u}_\mathrm{L}, \boldsymbol{v}_\mathrm{L})$.

To incorporate input delays, the delayed input $\boldsymbol{u}_{k,\text{del}}$ replaces $\boldsymbol{u}_k$ at each time step k

$$\boldsymbol{u}_{k,\text{del}} = \left[u_{1,k-N_{\text{d,r}}}, u_{2,k-N_{\text{d,j}}}\right]^{\text{T}}, \tag{12}$$

with $N_{\text{d,r}} = \frac{t_{\text{d,r}}}{\Delta t}$, $N_{\text{d,j}} = \frac{t_{\text{d,k}}}{\Delta t}$.

III. Kalman Filter Design

Only a subset of system states is directly measurable, and available sensor data are affected by noise. To enable state feedback control, a Kalman filter is employed, reconstructing the state vector from noisy measurements in real time.

We assume additive, uncorrelated Gaussian noise with zero mean for the process and measurement noise, described by covariance matrices $\boldsymbol{Q}$ and $\boldsymbol{R}$, respectively.

The Kalman filter algorithm starts with a prediction of the state $\hat{\boldsymbol{x}}_{k,\text{pred}}$ at time step k, based on the previous estimate$\hat{\boldsymbol{x}}_{k-1}$, input $\boldsymbol{u}_{k-1}$, disturbance $\boldsymbol{v}_{k-1}$, and linearization term $\boldsymbol{F}$

$$\begin{aligned}\hat{\boldsymbol{x}}_{k,\text{pred}} &= \boldsymbol{A}_{\text{d}}\hat{\boldsymbol{x}}_{k-1} + \boldsymbol{B}_{\text{u,d}}\boldsymbol{u}_{k-1} + \boldsymbol{B}_{\text{v,d}}\boldsymbol{v}_{k-1} \\ &\quad + \boldsymbol{F}(\boldsymbol{x}_{\text{L}}, \boldsymbol{u}_{\text{L}}, \boldsymbol{v}_{\text{L}}),\end{aligned} \tag{13a}$$

$$\boldsymbol{P}_{k,\text{pred}} = \boldsymbol{A}_{\text{d}}\boldsymbol{P}_{k-1}\boldsymbol{A}_{\text{d}}^{\text{T}} + \boldsymbol{Q}. \tag{13b}$$

The correction step updates the state estimate $\hat{\boldsymbol{x}}_k$ using the current measurement $\boldsymbol{y}_k$ and disturbance $\boldsymbol{v}_k$

$$\boldsymbol{K}_k = \boldsymbol{P}_{k,\text{pred}}\boldsymbol{C}^{\text{T}}(\boldsymbol{C}\boldsymbol{P}_{k,\text{pred}}\boldsymbol{C}^{\text{T}} + \boldsymbol{R})^{-1}, \tag{14a}$$

$$\hat{\boldsymbol{x}}_k = \hat{\boldsymbol{x}}_{k,\text{pred}} + \left(\boldsymbol{y}_k - \boldsymbol{C}\hat{\boldsymbol{x}}_{k,\text{pred}} - \boldsymbol{D}_{\text{v}}\boldsymbol{v}_k\right), \tag{14b}$$

$$\boldsymbol{P}_k = \left(\boldsymbol{I}_x - \boldsymbol{K}_k\boldsymbol{C}\right)\boldsymbol{P}_{k,\text{pred}}. \tag{14c}$$

Estimated states are denoted with a circumflex (ˆ).

IV. Linear Discrete MPC Design

For MPC objective design, the following terms are formulated for tracking of the variables T_{r}, $T_{\text{out,j}}$ and P at time step k and prediction step i

$$J_{\text{r},k,i} = q_{\text{r}}^2\left(\frac{y_{1,i} - y_{1,\text{ref},k+i}}{y_{1,\text{ref},k+i}}\right)^2, \tag{15}$$

$$J_{\text{j},k,i} = q_{\text{j}}^2\left(\frac{y_{2,i} - y_{2,\text{ref},k+i}}{y_{2,\text{ref},k+i}}\right)^2, \tag{16}$$

$$J_{\text{p},k,i} = q_{\text{p}}^2\left(\frac{P_i - P_{\text{ref},k+i}}{P_{\text{ref},k+i}}\right)^2, \tag{17}$$

where $y_{1,\text{ref}}$, $y_{2,\text{ref}}$, and P_{ref} represent the respective reference values for T_{r}, $T_{\text{out,j}}$, and P. The weighting factors q_{r}, q_{j} and q_{p} weight and scale the objective terms.

These objective terms represent the control goals: J_{r} constrains T_{r} below $100\,^{\circ}\text{C}$ for safety, J_{j} tracks $T_{\text{out,j}}$ ($\approx 50\,^{\circ}\text{C}$) for compatibility with the buffer storage connecting the reactor to the heating network, and J_{p} regulates P to meet short-term heating demand in future building applications.

As a benchmark for MPC, a PID controller has been designed in [11]. It consists of two decoupled SISO control loops for (u_1, y_1) and (u_2, y_2), neglecting all other input-output couplings.

Four different MPC objectives are investigated, as proposed in [11]

① tracking T_{r} and $T_{\text{out,j}}$: $J_{1,k,i} = J_{\text{r},k,i} + J_{\text{j},k,i}$
② tracking $T_{\text{out,j}}$: $J_{2,k,i} = J_{\text{j},k,i}$
③ tracking P: $J_{3,k,i} = J_{\text{p},k,i}$
④ tracking P and $T_{\text{out,j}}$: $J_{4,k,i} = J_{\text{j},k,i} + J_{\text{p},k,i}$

Objective ① regulates both T_{r} and $T_{\text{out,j}}$, enabling direct performance comparison with PID. Since T_{r} mainly acts as a constraint rather than a primary control target, objective ② narrows the focus to $T_{\text{out,j}}$. To explicitly address thermal output, objective ③ tracks P, while objective ④ blends objectives ② and ③ with temperature control and heat transfer.

To ensure safety, constraints for the outputs y_1 and y_2 are needed. Hard constraints may cause infeasibility due to input delays, disturbances, and numerical errors. Therefore, soft constraints are used, allowing deviations from limits, which are penalized in the objective function

$$J_{\text{c},k,i} = q_{\text{r}}^2\left(\frac{c_{1,i}}{y_{1,\text{ref},k+i}}\right)^2 + q_{\text{j}}^2\left(\frac{c_{2,i}}{y_{2,\text{ref},k+i}}\right)^2. \tag{18}$$

Therein, slack variables c_1 and c_2 adjust the outputs within limits

$$x_1(t) + c_1(t) \geq y_{1,\text{mean}} - y_{1,\text{dev}}, \tag{19a}$$

$$x_1 - c_1 \leq y_{1,\text{mean}} + y_{1,\text{dev}}, \tag{19b}$$

$$2x_2 + c_2 \geq v_3 + y_{2,\text{mean}} - y_{2,\text{dev}}, \tag{20a}$$

$$2x_2 - c_2 \leq v_3 + y_{2,\text{mean}} + y_{2,\text{dev}}, \tag{20b}$$

with mean values $y_{1/2,\text{mean}} = (y_{1/2,\text{max}} + y_{1/2,\text{min}})/2$ and deviations $y_{1/2,\text{dev}} = (y_{1/2,\text{max}} - y_{1/2,\text{min}})/2$. The outputs are permitted to violate their bounds $y_{1/2,\text{min}}$ and $y_{1/2,\text{max}}$ by up to $c_{1/2}$, maintaining feasibility without significant constraint violation.

In [11], a rate constraint was applied to u_2 to limit large changes, which occurred due to input delays, pump dynamics, and disturbances. However, this constraint was not effective, as u_2 still showed significant changes within its boundaries. To improve this, the current work explicitly penalizes changes in u_2 within the objective function at prediction step i

$$J_{\text{u},i} = q_{\text{u}}^2\left(\frac{u_{2,i} - u_{2,i-1}}{u_{2,\text{max}}}\right)^2, \tag{21}$$

with normalization to the maximum value $u_{2,\text{max}}$ of u_2 and scaling q_{u}.

Combining all objectives, the MPC optimization problem at time step k, $t = k\Delta t$, is

$$\min_{\tilde{\boldsymbol{U}}_1, \tilde{\boldsymbol{U}}_2, \tilde{\boldsymbol{C}}} \quad \sum_{i=N_{\text{d,j}}}^{N+1} J_{1/2/3/4,k,i} + J_{\text{c},k,i} + \sum_{i=0}^{N-N_{\text{d,j}}} J_{\text{u},i}, \tag{22a}$$

$$\text{s.t.} \quad \tilde{\boldsymbol{x}}(0) = \hat{\boldsymbol{x}}_k, \tag{22b}$$

$$\begin{aligned}\tilde{\boldsymbol{x}}_{i+1} &= \boldsymbol{A}_{\text{d}}\tilde{\boldsymbol{x}}_i + \boldsymbol{B}_{\text{u,d}}\tilde{\boldsymbol{u}}_{i,\text{del}} + \boldsymbol{B}_{\text{v,d}}\tilde{\boldsymbol{v}} \\ &\quad + \boldsymbol{F}(\boldsymbol{x}_{\text{L}}, \boldsymbol{u}_{\text{L}}, \boldsymbol{v}_{\text{L}}),\ i = 0, ..., N,\end{aligned} \tag{22c}$$

$$\tilde{\boldsymbol{y}}_i = \boldsymbol{C}\tilde{\boldsymbol{x}}_i + \boldsymbol{D}_{\text{v}}\tilde{\boldsymbol{v}}_i, \qquad i = 0, ..., N+1, \tag{22d}$$

$$\boldsymbol{x}_{\text{min}} \leq \tilde{\boldsymbol{x}} \leq \boldsymbol{x}_{\text{max}}, \quad i = N_{\text{d,j}}, ..., N+1, \tag{22e}$$

$$\boldsymbol{c}_{\text{min}} \leq \tilde{\boldsymbol{c}} \leq \boldsymbol{c}_{\text{max}}, \quad i = N_{\text{d,j}}, ..., N+1, \tag{22f}$$

$$\boldsymbol{u}_{\text{min}} \leq \tilde{\boldsymbol{u}} \leq \boldsymbol{u}_{\text{max}}, \quad i = 0, ..., N - N_{\text{d,j}}. \tag{22g}$$

The optimization yields the optimal input sequences $\tilde{\boldsymbol{U}}_1^* = [\tilde{u}_{1,0}^*, ..., \tilde{u}_{1,N-N_{\mathrm{d,r}}}^*]$, $\tilde{\boldsymbol{U}}_2^* = [\tilde{u}_{2,0}^*, ..., \tilde{u}_{2,N-N_{\mathrm{d,j}}}^*]$, and the optimal slack variables $\tilde{\boldsymbol{C}}^* = [\tilde{\boldsymbol{c}}_{N_{\mathrm{d,j}}}^*, ..., \tilde{\boldsymbol{c}}_{N+1}^*]$, with $\tilde{\boldsymbol{c}} = [\tilde{c}_1, \tilde{c}_2]^{\mathrm{T}}$. Symbols marked with a tilde ($\tilde{}$) denote predicted values over the prediction horizon N.

The optimization is subject to the system dynamics (22c), the output equation (22d), and the state, input, and slack variable constraints (22e)-(22f), including the additional soft constraints (19) and (20). The state is initialized with the estimated state $\hat{\boldsymbol{x}}_k$ at time step k. The disturbance is assumed constant over the prediction horizon, i.e., $\tilde{\boldsymbol{v}} = \boldsymbol{v}_k$.

To account for the input delays, the prediction also incorporates the previously applied optimal inputs $u_{1,k-N_{\mathrm{d,r}}}^*, ..., u_{1,k-1}^*$ and $u_{2,k-N_{\mathrm{d,j}}}^*, ..., u_{2,k-1}^*$.

Since $N_{\mathrm{d,j}} < N_{\mathrm{d,r}}$ is known for this system, the objective function is formulated in terms of $N_{\mathrm{d,j}}$. Otherwise, it would depend on $\min\{N_{\mathrm{d,r}}, N_{\mathrm{d,j}}\}$.

For MPC, only the first element of the computed input sequences is applied to the system, i.e., $\tilde{u}_{1,0}^*$ and $\tilde{u}_{2,0}^*$. However, the input $\tilde{u}_1$, treated as continuous in the optimization, can only be actuated as a binary (on/off) signal. Therefore, a peak-matching pulse width modulation, introduced in [11], is used to convert the optimized sequence $\tilde{\boldsymbol{U}}_1^*$ into a binary control signal. This method centers the high phase of the pulse around the original maximum of the windowed sequence. The first element of the resulting signal is then applied to the system as $u_{1,k}^*$. Input u_2 is directly applied $u_{2,k}^* = \tilde{u}_{2,0}^*$.

V. Simulation Results

This section presents simulation results for MPC using different control objectives. It begins with an analysis of the Kalman Filter performance, followed by comparisons between the control objectives and between linear discrete-time MPC with observer and both nonlinear and linear continuous-time MPC with full-state feedback.

The simulation uses a sampling time of $\Delta t = 1\,\mathrm{s}$, matching the experimental setup.

Initial results confirm that updating the linearization point $(\boldsymbol{x}_{\mathrm{L}}, \boldsymbol{u}_{\mathrm{L}}, \boldsymbol{v}_{\mathrm{L}})$ is essential to maintain model accuracy. Especially with further material conversion and resulting changes in heat capacity and total material mass. At time step k, the following points are chosen: $\boldsymbol{x}_{\mathrm{L}} = \hat{\boldsymbol{x}}_k$, $\boldsymbol{v}_{\mathrm{L}} = \boldsymbol{v}_k$, $\boldsymbol{u}_{\mathrm{L}} = \boldsymbol{u}_{\min}$. This choice reflects that for u_1, only $u_{1,\min}$ yields a linearization with good model fit. This may be due to $u_1 = u_{1,\min} = 0$ being a stationary input, whereas $u_1 > 0$ always initiates reaction. For u_2, an updated linearization point could be chosen, but does not affect the performance significantly.

Optimization is performed in MATLAB using CasADi's nlpsolve with IPOPT, allowing direct comparison with the nonlinear MPC in [11]. For real-time implementation in Simulink, quadratic solvers such as qpOASES are suitable.

A. State Estimation

In [11], measurement noise was not explicitly considered in the system model. In this study, measurement noise is incorporated as Gaussian normal distributed additive noise

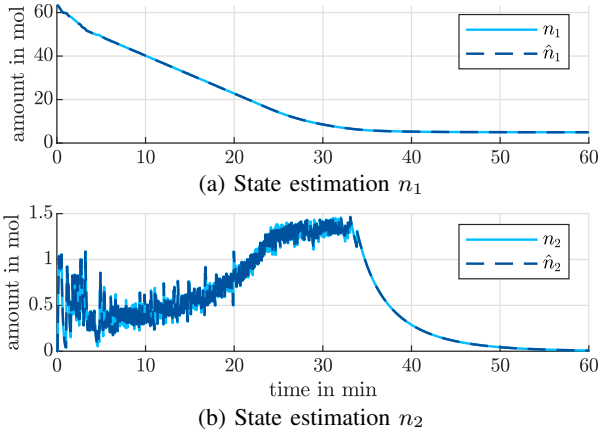

(a) State estimation n_1

(b) State estimation n_2

Fig. 4: State estimates $\hat{n}_1$, $\hat{n}_2$ and actual states n_1, n_2.

TABLE IV: Observer performance for experiments and mean values.

	①	②	③	④	mean
RMSE T_{r} (K)	0.032	0.034	0.032	0.039	0.034
RMSE $T_{\mathrm{out,j}}$ (K)	0.030	0.029	0.030	0.029	0.030
RMSE n_1 (mol)	0.043	0.100	0.054	0.143	0.085
RMSE n_2 (mol)	0.0076	0.0082	0.0066	0.0117	0.0085
RMSE x_{u2} (l/h)	0.091	0.091	0.091	0.091	0.091

at the system outputs. In accordance with measured signal values, the standard variances $\sigma_{\mathrm{T,r}}^2 = \sigma_{\mathrm{T,j}}^2 = 10^{-2}$ and $\sigma_{\mathrm{T,u2}}^2 = 10^{-9}$ were chosen for the temperature outputs T_{r} and $T_{\mathrm{out,j}}$ and the cooling mass flow x_{u2}.

For the Kalman Filter, the measurement noise covariance matrix was set to $\boldsymbol{R} = \mathrm{diag}(10^{-2}, 10^{-2}, 10^{-9})$, matching the variance of the simulated measurement noise.

For simplicity, $\boldsymbol{Q}$ is set as a diagonal matrix $\boldsymbol{Q} = \mathrm{diag}(10^{-4}, 10^{-4}, 10^{-4}, 10^{-5}, 10^{-8})$. This choice reflects a higher confidence in the system model than the output measurement to smooth the output noise for states T_{r}, T_{j}, n_1 and n_2. For n_2 the value was reduced by factor 10, to account for the smaller magnitude of the state. For x_{u2}, a larger variance was selected for process noise compared to measurement noise, resulting in less filtering and greater reliance on the output. Although x_{u2} is smoothed by the penalty on u_2, it still exhibits dynamic behavior that exceeds the magnitude of the measurement noise. Consequently, the observer design prioritizes responsiveness to the output dynamics over noise filtering.

The initial guess for $\boldsymbol{P}$ is $\boldsymbol{P}_0 = 10^{-10}\boldsymbol{I}_x$, since $\hat{\boldsymbol{x}}_0 = \boldsymbol{x}_0$, the set of initial conditions for the observer, is initialized with measured values and therefore accurate.

Results for objective ② for the states n_1 and n_2 are shown in Fig. 4. The plot confirms that the estimated states closely follow the true system behavior. Table IV summarizes the root mean square error (RMSE) and its mean value for all states across the four MPC objectives. The RMSE for T_{r} and $T_{\mathrm{out,j}}$ lies below the measurement noise standard deviation ($\sigma_{\mathrm{T,r}} = \sigma_{\mathrm{T,j}} = 10^{-1}\,(^\circ\mathrm{C})$), indicating high estimation accuracy. For x_{u2}, the RMSE approximately matches the noise level ($(0.91\,\mathrm{l/h})^2 = 6.4\times10^{-10}\,(\mathrm{kg/s})^2 \approx 1\times10^{-9}\,(\mathrm{kg/s})^2$), which is consistent with the Kalman Filter design.

B. Control

This section presents simulation results for the different MPC objectives with Kalman filter, and compares linear discrete MPC with observer to nonlinear and linear continuous MPC with full-state feedback. A prediction horizon of 20 s ($N = 20$) is used, matching our prior work.

Input and state constraints, as well as initial conditions and disturbances, are identical to those used in [11]. As in the previous work, the reactor contained 4.1 kg of material.

The control setpoints are a reactor temperature of 90 °C, a cooling water outlet temperature of 50 °C and a thermal output of 1.5 kW. These also serve as normalization values for c_1 and c_2 when no reference trajectory is specified.

The weightings q are set to $q_\mathrm{r} = q_\mathrm{j} = q_\mathrm{p} = 10$ to improve numerical conditioning. The weighting $q_\mathrm{u} = 3$ balances the influence of the rate constraint relative to the other objectives. A higher value would overly restrict the control input u_2, resulting in slower system response and overshooting. The chosen value represents a compromise between enforcing input smoothness and maintaining tracking performance.

1) Comparison of MPC objectives with state observer: The results for the different MPC objectives are given in Fig. 5 and Tabs. V, VI.

During warm-up (0-5 min), controllers that include tracking of T_r (①, PID) exhibit a slower rise in reactor temperature, as they follow the reference. Controllers that do not track T_r (②-④) allow for a rapid temperature increase. This is driven by the need to raise $T_\mathrm{out,j}$ quickly, either for direct temperature tracking (②) or to achieve the desired output power (③) or both (④). These differences are also reflected in the cooling water mass flow. A slower reactor temperature rise (①, PID) requires a lower cooling water flow to allow $T_\mathrm{out,j}$ to increase. Consequently, thermal output power rises more slowly for these controllers compared to others.

During the tracking phase (5-25 min), all controllers achieve good performance with respect to their respective objectives. MPC ① outperforms PID in terms of tracking quality, benefiting from model-based prediction and the smoothing effect of state estimation. For $T_\mathrm{out,j}$, which is influenced by the disturbance $T_\mathrm{in,j}$, all controllers exhibit some residual noise.

The implementation of the rate constraint on u_2 was effective, reducing set point changes in the input signal. The selected weighting q_u successfully balances responsiveness with input smoothness. Compared to NMPC in previous work [11], the new constraint implementation leads to different set points for the controllers, such that the cool down phase is reached 5 min earlier (before: 30 min).

In the cool-down phase (25-60 min), controllers that include power tracking (③, ④) increase the cooling water flow to maximize energy extraction, which causes an earlier decrease in $T_\mathrm{out,j}$. Although the final output power levels are very similar across all objectives, ③ and ④ provide considerably higher cumulative cooling water consumption over the course of the experiment.

Tables V and VI summarize RMSE, energy output, and computation time for the first 25 minutes and the full

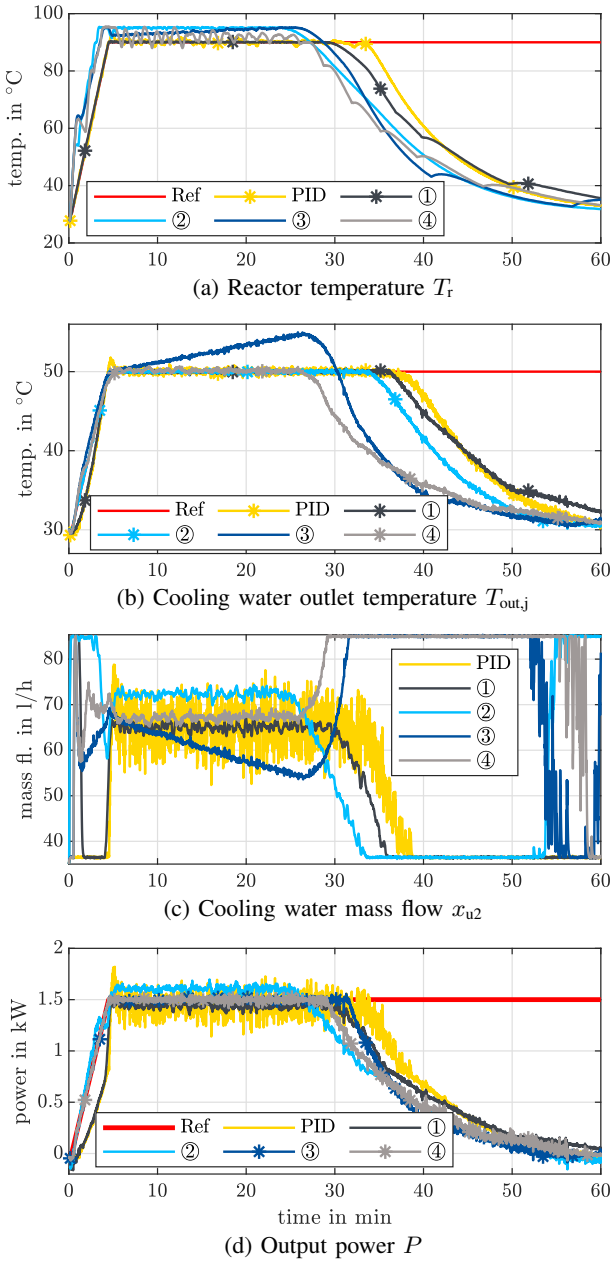

(a) Reactor temperature T_r

(b) Cooling water outlet temperature $T_\mathrm{out,j}$

(c) Cooling water mass flow x_u2

(d) Output power P

Fig. 5: System simulation with different MPC and PID. Only marked $*$ lines are with tracking.

experiment. MPC ② achieves the highest average power output during the first 25 minutes due to its high cooling water mass flow rate. However, ③ and ④ use the most water overall due to their cool down behavior.

Controllers with single tracking objectives generally perform better for their respective targets, i.e., ② for $T_\mathrm{out,j}$ and ③ for power, compared to those that combine multiple goals.

2) Comparison of different MPC models: The linear discrete MPC with observer is compared to MPC variants using different models and full state information without noise. All variants apply objective ①. Three approaches are evaluated: nonlinear continuous-time MPC (NMPC), linear continuous-time MPC (LMPC), and linear discrete-time MPC (LDMPC). The results are shown in Tab. VII.

TABLE V: Comparison of controller approaches for 0-25 min of experiment. TCWM: total cooling water mass, Time: total computation time.

	①	②	③	④	PID
RMSE T_r (K)	0.3	-	-	-	0.8
RMSE $T_\mathrm{out,j}$ (K)	1.0	0.1	-	0.4	1.1
RMSE P (W)	-	-	18.1	19.8	-
J (kW h)	0.514	0.603	0.564	0.564	0.514
TCMW (kg)	26.0	30.6	25.3	27.8	25.0
Time (min)	6.7	6.4	6.7	7.6	0.0005

TABLE VI: Comparison of controller approaches. TCWM: total cooling water mass, Time: total computation time.

	①	②	③	④	PID
RMSE T_r (K)	28.2	-	-	-	28.7
RMSE $T_\mathrm{out,j}$ (K)	8.0	9.7	-	11.0	8.5
RMSE P (W)	-	-	858.9	832.4	-
J (kW h)	0.877	0.882	0.876	0.877	0.897
TCMW (kg)	51.3	59.3	67.6	74.7	51.4
Time (min)	16.4	15.5	16.0	18.1	0.0008

Across all models, tracking performance during the first 25 minutes is equally good. The most significant differences lie in computation time. LDMPC requires 4 % less computation time than NMPC and even more for LMPC. Computation times for LDMPC can be lowered by directly using specialized solvers for quadratic optimization such as qpOASES or OSQP, rather than using nlpsolve (CasADi) with IPOPT.

VI. Conclusion and Outlook

In this work, a state observer and a model predictive controller were developed based on a linearized time-discrete model of a thermochemical energy storage system. Building on [11], the nonlinear model was linearized and discretized to enable its use in both a Kalman filter for state estimation and as prediction model within the MPC framework.

Four MPC objectives were investigated, focusing on tracking the reactor temperature, cooling water outlet temperature, and thermal output power. The state feedback loop was closed by the Kalman filter, which provided estimates for unmeasured states. The filter showed high accuracy in reconstructing the full state and effectively reduced measurement noise, confirming its suitability for use within the MPC. The introduced rate constraint on input u_2 successfully prevented excessive set point changes. All MPC objectives achieved good tracking performance. Among these, ②, targeting the cooling water outlet temperature $T_\mathrm{out,j}$, offers the best computational efficiency. If thermal output power must also be considered, ④, including both $T_\mathrm{out,j}$ and the output power P, is suitable, but at the cost of increased computation time. Nevertheless, all evaluated MPC variants are applicable for real-time implementation.

Comparing the linear discrete-time MPC with state observer to a nonlinear continuous-time MPC with full state information, no significant loss in control performance was observed. At the same time, computation time was reduced.

The next step is the integration of the linear discrete-time MPC and Kalman filter into the experimental setup. This includes implementation in Simulink with solver qpOASES, code generation, and deployment to the PLC for conduction of experiments.

TABLE VII: Comparison of MPC with different simulation models for 0-25 min/full experiment, without state estimation and noise.

	NMPC	LMPC	LDMPC
RMSE T_r (K)	0.3/28.6	0.3/28.4	0.3/28.4
RMSE $T_\mathrm{out,j}$ (K)	1.0/8.2	1.0/8.1	1.0/8.1
J (kW h)	0.514/0.872	0.514/0.875	0.514/0.875
TCMW (kg)	25.9/51.2	26.0/51.3	26.1/51.3
Time (min)	7.0/16.7	6.9/17.2	6.6/16.1

Acknowledgment

The authors used OpenAI's ChatGPT to assist with language editing during manuscript preparation. All content was manually approved.

References

[1] International Energy Agency, "Heating," Paris, 2025, accessed: 29.07.2025. [Online]. Available: https://www.iea.org/energy-system/buildings/heating

[2] V. Kühl, M. Linder, and M. Schmidt, "Experimental Study on Heat Recovery in a CaO/Ca(OH)2-Based Mechanical Fluidized Bed Thermochemical Energy Storage Reactor," *Energies*, vol. 17, no. 19, p. 4770, 2024.

[3] M. Schmidt, V. Sourmelis, V. Kühl, and M. Linder, "Zero emission heating with calcium oxide and water: development and demonstration of first pilot scale thermochemical heating system for buildings," *Frontiers in Energy Research*, vol. 13, 2025.

[4] J. W. Eaton and J. B. Rawlings, "Feedback control of chemical processes using on-line optimization techniques," *Computers & Chemical Engineering*, vol. 14, no. 4-5, pp. 469–479, 1990.

[5] F. Xaumier, B. Ettedgui, M.-V. Le Lann, M. Cabassud, and G. Casamatta, "Non-linear model predictive control for thermal control of a semi-batch reactor: Experimental and simulation results," in *1999 European Control Conference (ECC)*. IEEE, 1999, pp. 1434–1439.

[6] R. E. Kalman, "A New Approach to Linear Filtering and Prediction Problems," *Journal of Basic Engineering*, vol. 82, no. 1, pp. 35–45, 1960.

[7] G. Welch and G. Bishop, "An Introduction to the Kalman Filter," University of North Carolina, Department of Computer Science, Chapel Hill, NC, USA, Chapel Hill, NC, USA, 1995.

[8] P. de Valliere and D. Bonvin, "Application of estimation techniques to batch reactors - II. Experimental studies in state and parameter estimation," *Computers & Chemical Engineering*, vol. 13, no. 1-2, pp. 11–20, 1989.

[9] M. A. Myers and R. H. Luecke, "Process control applications of an extended Kalman filter algorithm," *Computers & Chemical Engineering*, vol. 15, no. 12, pp. 853–857, 1991.

[10] N. L. Ricker and J. H. Lee, "Nonlinear modeling and state estimation for the Tennessee Eastman challenge process," *Computers & Chemical Engineering*, vol. 19, no. 9, pp. 983–1005, 1995.

[11] A. Rentz, V. E. Sourmelis T., V. Kühl, M. Schmidt, M. Linder, and O. Sawodny, "Model Predictive Control of the Hydration Process In a Lime-Based Thermochemical Energy Storage System," *Journal of Dynamic Systems, Measurement, and Control*, pp. 1–15, 2025.

[12] J. H. Lee and A. K. Datta, "Nonlinear inferential control of pulp digesters," *AIChE Journal*, vol. 40, no. 1, pp. 50–64, 1994.

[13] T. F. Finkler, M. Kawohl, U. Piechottka, and S. Engell, "Realization of online optimizing control in an industrial semi-batch polymerization," *Journal of Process Control*, vol. 24, no. 2, pp. 399–414, 2014.

[14] D. Haßkerl, S. Subramanian, S. Markert, S. Kaiser, and S. Engell, "Multi-rate state estimation applied to a pilot-scale reactive distillation process," *Chemical Engineering Science*, vol. 185, pp. 256–281, 2018.

[15] A. Kummer, L. Nagy, and T. Varga, "NMPC-based control scheme for a semi-batch reactor under parameter uncertainty," *Computers & Chemical Engineering*, vol. 141, p. 106998, 2020.

[16] A. Rentz, V. Kühl, V. E. Sourmelis T., M. Schmidt, M. Linder, O. Sawodny, and M. Böhm, "Modeling and Identification of the Hydration Process in a CaO/Ca(OH)2-based Heat Storage System," *at - Automatisierungstechnik*, vol. 71, no. 8, pp. 584–598, 2023.